Progress of Theoretical Physics, Vol. 117, No. 6, June 2007

A Formation Mechanism of Collapsar Black Hole

—— *Early Evolution Phase* ——

Yuichiro Sekiguchi and Masaru Shibata

Graduate School of Arts and Sciences, University of Tokyo, Tokyo 153-8902, Japan

(Received February 27, 2007)

The latest studies of massive star evolution indicate that an initially rapidly rotating star with sufficiently low metallicity can produce a rapidly rotating, massive stellar core that could be a progenitor of long-soft gamma-ray bursts (LGRBs). Motivated by these studies, we follow the collapse of a rapidly rotating massive stellar core to a 'collapsar' black hole (BH) surrounded by a massive, hot accretion disk performing fully general relativistic simulations. We focus on the general relativistic dynamics of the collapse, and the relevant microphysics is treated in a qualitative manner. The simulations are performed until the system consisting of the BH and the disk has relaxed to a quasi-stationary state. A novel mechanism found in this study is that strong shock waves are formed at the inner part of the disk after the formation of the BH. These shock waves propagate mainly along the rotation axis, heating the disk and sweeping materials around the rotational axis, and thereby forming a low density region. The temperature of the disk is high enough for copious neutrino emission. All these features indicate that the direct formation of a rapidly rotating BH is a promising source of LGRBs even in the absence of strong magnetic fields.

§1. Introduction

The observed association of afterglows of long gamma-ray bursts (LGRBs) with star forming regions in galaxies,[1)–3)] such as the connections between GRB980425 and the Type Ib/c supernova SN1998bw,[4),5)] between GRB030329 and the Type Ic supernova SN2003dh,[6)–8)] and between GRB060218 and the Type Ic supernova SN2006aj,[9),10)] (see also Ref. 11) for other suggested associations between LGRBs and core-collapse supernovae), suggested that at least some LGRBs are associated with supernovae and the core collapse of massive stars. Supported by this evidence, the collapsar scenario, in which the central engine of LGRBs is composed of a rotating black hole (BH) surrounded by a massive, hot accretion disk,[12)–14)] is currently the most favored model for LGRBs. It requires the progenitors to be rotating rapidly enough that an accretion disk can be formed around the BH. Also, the relativistic jets that are to produce the LGRB have to reach the stellar surface. This constrains the size of the progenitor; the progenitor should not have an extended hydrogen envelope.[14),15)] Thus, the progenitors of LGRBs are now believed to be rapidly rotating massive Wolf-Rayet (WR) stars.

However, WR stars are known to be accompanied by strong stellar winds driven by radiation pressure which lead to a rapid spin-down of the cores of the WR stars.[16)] Some authors[17),18)] have proposed binary-evolution models for producing rapidly rotating progenitors of LGRBs. On the other hand, Yoon and Langer and Woosley and Heger have recently discovered[19)–21)] that even a single star can fulfill the re-

quirements of the collapsar scenario if it is initially rapidly rotating ($\gtrsim 50\%$ of the Keplerian velocity at the equatorial surface) and of low metallicity ($Z/Z_\odot \lesssim 0.1$). The mass loss is suppressed by the low metallicity.[22] The rapid rotation results in a short mixing timescale, which leads to a chemically homogeneous state throughout the hydrogen burning phase.[23] In this case, a single star can become a rapidly rotating WR star without losing the hydrogen envelope through the stellar wind, avoiding the red giant phase that otherwise would cause a significant decrease of the core angular momentum due to magnetic torques.[19),20]

In addition to the above single-star evolutionary scenario to the LGRB progenitor, recent growing empirical evidence indicates that LGRBs may prefer a low metallicity environment.[24)–27] At least some LGRBs are likely to be formed from a rapidly rotating WR star which is born in a low metallicity environment and experiences chemically homogeneous evolution.

Motivated by these latest studies, we perform axisymmetric simulations of rapidly rotating stellar core collapse to a BH in full general relativity. We explore the outcome of the collapse of very massive, rapidly rotating WR stars in the context of the collapsar scenario. As a first step toward more realistic simulations, microphysical processes are treated only in a qualitative manner, focusing on the general relativistic hydrodynamics of the collapse. Throughout this paper, c and G denote the speed of light and the gravitational constant, respectively.

§2. Setting

To model the core of WR stars just before the collapse, we adopt the polytropic equation of state (EOS) $P = K\rho^\Gamma$, with $\Gamma = 4/3$, taking account of degenerate electron and radiation pressures. Here K is a constant. Rigid rotation is adopted as the rotation profile for simplicity. The maximum angular velocity (which is equal to the Kepler angular velocity of the equatorial surface) is assumed, since the progenitor (a WR star) of LGRBs is likely to be rapidly rotating. The central density and temperature of a pre-collapse iron core of massive metal-poor stars are $\rho_c \gtrsim 10^9$ g/cm^3 and $T_c \lesssim 10^{10}$ K (according to Umeda and Nomoto). We set the central density of the initial conditions to $\rho_c \approx 5 \times 10^9$ g/cm^3. Note that the chemical potential of the electrons at such a density is larger than the temperature $T \approx 10^{10}$ K, and hence the electrons are degenerate even at such a high temperature.

According to the latest models of stellar evolution,[19)–21] rapid rotation results in a chemically homogeneous state and leads to a large CO core which could produce an iron core with mass $\gg 2M_\odot$.[21] The CO core mass $M_{\rm CO}$ can be approximately 10, 17, $25M_\odot$ for models of initial mass 20, 30, $40M_\odot$, according to the result of Ref. 20). Taking this fact into account, we choose models with a core mass of $M \approx 3.5$–$4.5M_\odot$. This is achieved by setting $K \approx 9$–10.5×10^{14} cm^3/s^2/g$^{1/3}$. [Note that the mass is approximately given by $4.555(K/G)^{3/2}$ for the $\Gamma = 4/3$ polytrope (see, e.g., Ref. 28)).] In this case, a BH is formed directly as a result of the collapse for any of the chosen EOSs (see the next paragraph). Because we have found qualitatively the same results for different mass models, we present the results for $M = 4.2M_\odot$ in the following. In this model, the ratio of the rotational kinetic energy $T_{\rm rot}$ to the

Table I. The parameter set (Γ_1,Γ_2,$\rho_{\rm nuc}$,$\Gamma_{\rm th}$), the maximum gravitational mass $M_{\rm max}$, and the time $t_{\rm AH}$ at which the first apparent horizon is formed.

Model	Γ_1	Γ_2	$\rho_{\rm nuc}$(g/cm^3)	$\Gamma_{\rm th}$	$M_{\rm max}$ ($M_\odot$)	$t_{\rm AH}$ (ms)
A	1.315	2.6	2.0×10^{14}	1.315	1.990	230
B	1.32	2.5	1.9×10^{14}	1.32	1.999	276
C	1.325	2.45	2.0×10^{14}	1.325	1.992	358

gravitational potential energy W is $T_{\rm rot}/|W| \approx 0.0088$. The nondimensional spin parameter $q \equiv cJ/GM^2$ is ≈ 0.98, where M and J denote the mass and angular momentum of the core, respectively.

For the evolution, we adopt a hybrid EOS (see, e.g., Ref. 29)) in which the pressure consists of the sum of cold and thermal parts, as $P = P_{\rm cold} + P_{\rm th}$, where

$$P_{\rm cold} = \begin{cases} K_1\rho^{\Gamma_1}, & \rho \le \rho_{\rm nuc}, \\ K_2\rho^{\Gamma_2}, & \rho \ge \rho_{\rm nuc}, \end{cases} \tag{2·1}$$

($\rho_{\rm nuc}$ denoting the nuclear density) and $P_{\rm th} = (\Gamma_{\rm th}-1)\rho(\varepsilon-\varepsilon_{\rm cold})$. Here, ρ is the rest-mass density, ε and $\varepsilon_{\rm cold}$ are the total and cold parts of the specific internal energy, Γ_1, Γ_2, and $\Gamma_{\rm th}$ are constants, $K_1 = 5\times10^{14}$ in cgs units, and $K_2 = K_1\rho_{\rm nuc}^{\Gamma_2-\Gamma_1}$, respectively. By choosing a value of Γ_1 slightly smaller than 4/3, the effect of the depletion of the degenerate electron pressure due to photo-dissociation and electron capture is qualitatively taken into account. The specific internal energy is set to the same value as in the case of the $\Gamma = 4/3$ polytropic EOS, i.e. $\varepsilon = 3K\rho^{1/3}$.

The values of Γ_1 are chosen as 1.315, 1.32, and 1.325 in this paper. For the case of ordinary supernova simulations (i.e. the collapse of a stellar core with a mass smaller than those in the present work), the value of Γ_1 may be in the range $1.30 \le \Gamma_1 \le 1.33$.[29] For the collapse of cores with larger masses, it has been pointed out that the value of Γ_1 tends to be larger than in the lower mass case, due to their larger entropies (see, e.g., Ref. 30)). For this reason, we believe that the values of Γ_1 adopted in this paper may be appropriate. The values of Γ_2 and $\rho_{\rm nuc}$ are chosen so that the maximum allowed gravitational mass of the cold neutron star is $M_{\rm max} \approx 2.0M_\odot$, which is approximately equal to the highest pulsar mass ever measured,[31] i.e., $M = 2.1 \pm 0.2M_\odot$. We set $\Gamma_{\rm th} = \Gamma_1$ for simplicity. With such small values, the low efficiency of the shock heating due to the energy loss through photo-dissociation and neutrino emission is qualitatively taken into account. The adopted values for the parameter set (Γ_1,Γ_2,$\rho_{\rm nuc}$,$\Gamma_{\rm th}$) are listed in Table I.

The temperature T is estimated from ε by solving the equation

$$\varepsilon = \varepsilon_{\rm gas} + \varepsilon_{\rm rad} + \varepsilon_\nu + \varepsilon_{\rm cold}\,, \tag{2·2}$$

where $\varepsilon_{\rm gas}$, $\varepsilon_{\rm rad}$, and ε_ν denote the specific internal energy of the gas, the radiation, and the neutrinos and are functions of ρ and T. We use the same forms for these quantities as in Ref. 32), setting

$$\varepsilon_{\rm gas} = \frac{3\rho kT}{2m_p}\frac{1+3X_{\rm nuc}}{4}, \tag{2·3}$$

$$\varepsilon_{\rm rad} = \frac{11}{4} a T^4, \tag{2·4}$$

$$\varepsilon_{\nu} = \frac{21}{8} a T^4 \Theta(\tau - \tau_{\rm crit}), \tag{2·5}$$

$$\varepsilon_{\rm cold} = \frac{hc}{24\pi^3} \left(\frac{3\pi^2 \rho Y_e}{m_p} \right)^{4/3}, \tag{2·6}$$

where k is the Boltzmann constant, h Planck's constant, m_p the nucleon mass, $X_{\rm nuc}$ the mass fraction of free nucleons, a the radiation constant, and Y_e the electron fraction. Further, Θ denotes the Heaviside step function; i.e., for an optical depth τ larger than the critical optical depth $\tau_{\rm crit} \approx 2/3$, we assume that the neutrinos are opaque with respect to nucleons and electrons and take into account their energy densities. (The definition of τ is given in §3.)

Simulations were performed using an axisymmetric, full general relativistic code.[33] The so-called simple excision technique[34] was implemented to follow the evolution of the BH spacetime in a stable manner. (For recent calculations, see, e.g., Refs. 35) and 36).) The regridding technique[37] was adopted during the collapse. The grid size and grid spacing in the final regridding were $(3300, 3300)$ for (ω, z) and $\Delta x \approx M/20$, where $\omega = \sqrt{x^2 + y^2}$ is the radius in cylindrical coordinates.

§3. Results

In the early stage, during which the central density of collapsing core is smaller than the nuclear density, the collapse proceeds in an approximately homologous manner. Then, as the central density approaches the nuclear density, the collapse around the equatorial plane is decelerated, due to the centrifugal force, while the collapse along the rotational axis is relatively accelerated to form a flattened structure. Since the mass of the stellar core is much larger than the maximum allowed mass for the given EOS, a BH is formed directly. The formation of the BH is ascertained by finding the apparent horizon. After the apparent horizon is formed (for the formation time, see Table I), a centrifugally supported, thin accretion disk is formed around the BH (see the top left panel of Fig. 1): The disk rotates at approximately the Keplerian velocity (see the bottom panel of Fig. 2). The evolution of the irreducible mass of the BH, $M_{\rm irr} \equiv \sqrt{A/16\pi}$, and the disk mass $M_{\rm disk}$ are shown in Fig. 3. Here A is the area of the apparent horizon.

After the disk formation, shocks are formed at the inner part of the disk, converting the kinetic energy of the infall into thermal energy (See Ref. 38) for discussion of a similar phenomenon.) The gravitational potential energy released is $E \sim G M_{\rm BH} M_{\rm disk}/R_{\rm ISCO} \approx 4$–$5 \times 10^{52}$ ergs, where $M_{\rm BH}$, $M_{\rm disk} \sim 0.1 M_\odot$, and $R_{\rm ISCO} \approx 4$–$5 G c^{-2} M_{\rm BH}$ are the black hole mass, the disk mass, and the radius of the innermost stable circular orbit around the BH, respectively. As the thermal energy is stored, the disk height H increases. For $H < R_{\rm ISCO}$, H in the vicinity of the BH is approximately determined by the balance relation

$$\frac{P_{\rm disk} - P_{\rm ram}}{H} \sim \frac{G M_{\rm BH} \rho_s H}{R_{\rm ISCO}^3}, \tag{3·1}$$

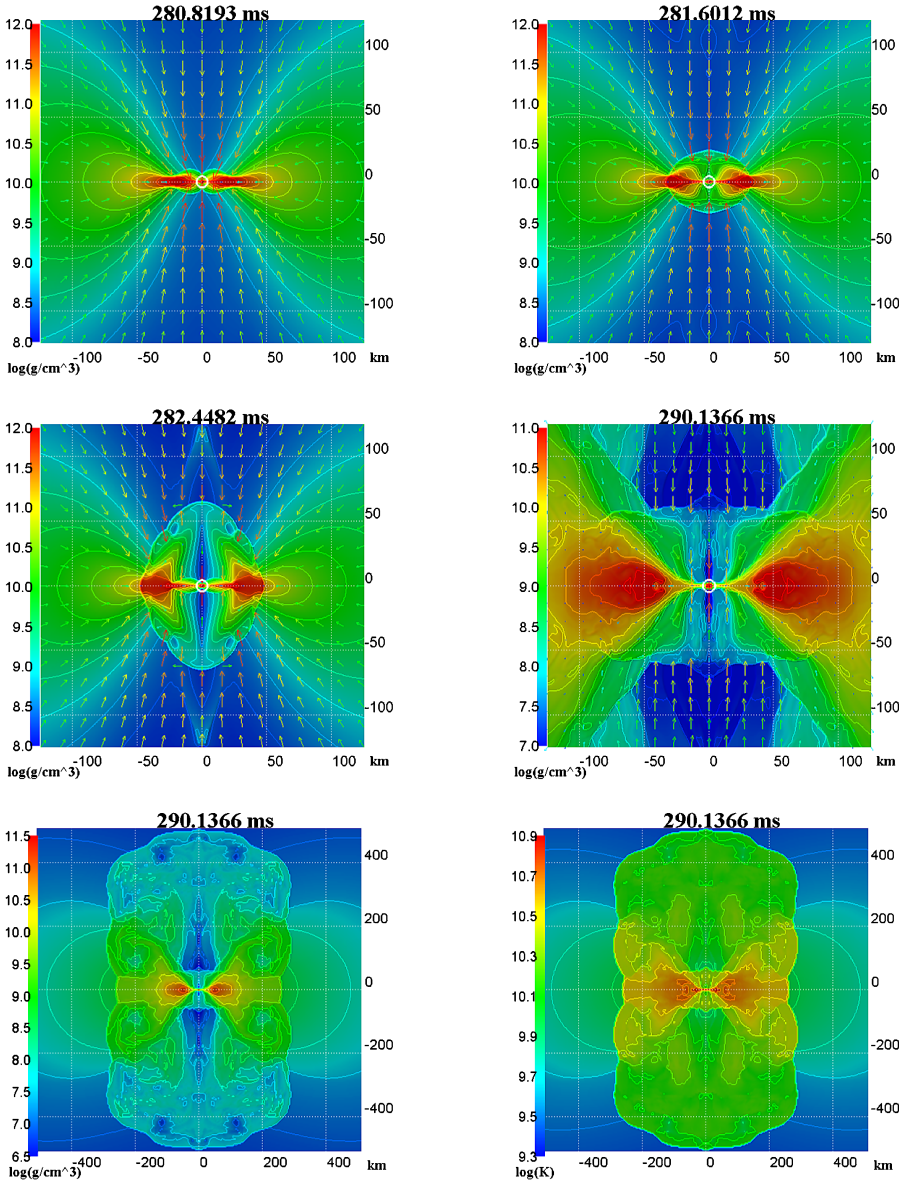

Fig. 1. Snapshots of density contours and velocity fields of the central region of the core in the x-z plane at $t \approx 280.82$ ms (the top left panel), 281.60 ms (the top right panel), 282.25 ms (the middle left panel), and 290.14 ms (the middle right panel). Snapshots of density contours (the bottom left panel) and temperature contours (the bottom right panel) in the x-z plane at 290.14 ms. All figures are for model B.

where the left-hand and right-hand sides represent the pressure gradient and the gravity of the BH. The quantities $\rho_{\rm s}$, $P_{\rm disk}$, and $P_{\rm ram}$ are the disk density near the surface, the pressure inside the disk, and the ram pressure of the infalling matter,

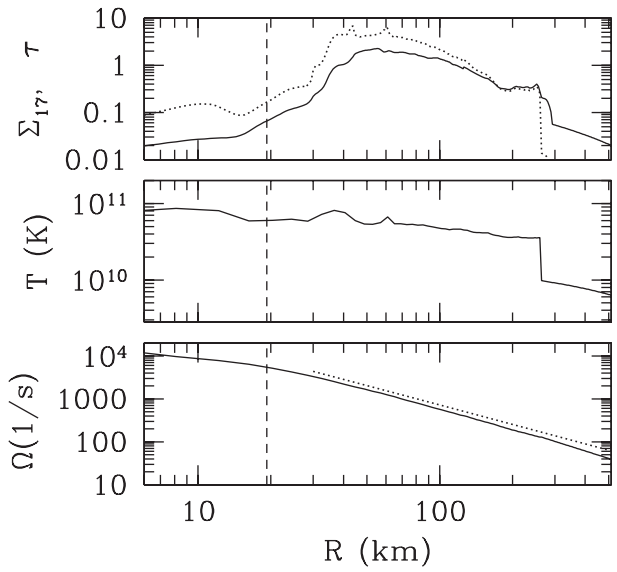

Fig. 2. Various quantities characterizing the disk at 290.14 ms for model B. The top panel plots the surface density $\Sigma_{17} \equiv \Sigma/10^{17}\mathrm{g/cm}^2$ (solid curve) and the optical depth $\tau \approx \kappa_\nu \Sigma$ (dotted curve). The middle panel plots the temperature evaluated in the equatorial plane. The bottom panel plots the angular velocity Ω (solid line) and the Keplerian angular velocity (dotted curve). The vertical dashed lines at $R \approx 19$ km indicate the expected location of the marginally stable circular orbit around the BH.

respectively. Equation (3·1) provides the order of magnitude of the pressure as

$$(P_{\rm disk} - P_{\rm ram}) \sim \frac{GM_{\rm BH}\rho_s H^2}{R_{\rm ISCO}^3} \sim 10^{31} \left(\frac{\rho_{\rm s}}{10^{11}{\rm g/cm}^3}\right) \left(\frac{H}{R_{\rm ISCO}}\right)^2 \ {\rm dyn/cm}^2. \quad (3\cdot2)$$

The ram pressure can be expressed as

$$P_{\rm ram} \sim \rho_{\rm f} v_{\rm f}^2 \sim 10^{30} \left(\frac{\rho_{\rm f}}{10^{10}\,{\rm g/cm}^3}\right) \ {\rm dyn/cm}^2, \quad (3\cdot3)$$

where $\rho_{\rm f}$ and $v_{\rm f} \sim (2GM_{\rm BH}/R_{\rm ISCO})^{1/2} \sim 0.4$–$0.5c$ are the density and velocity of the infalling matter.

The density ($\rho_{\rm disk}$) and the temperature ($T_{\rm disk}$) inside the disk eventually increase to $\sim 10^{12}$ g/cm^3 and $\sim 10^{11}$ K (and hence, $P_{\rm disk} \sim 10^{31}$ dyn/cm^2), while the ram pressure ($P_{\rm ram}$) decreases to $\lesssim 0.1 P_{\rm disk}$ ($\ll P_{\rm disk}$), since the density of the infalling matter ($\rho_{\rm f}$) decreases to $\lesssim 10^{10}$ g/cm^3. Consequently, H increases to $\sim R_{\rm ISCO}$ for $\rho_{\rm s} \sim 10^{11}$ g/cm^3. Then, the approximate balance relation becomes

$$(P_{\rm disk} - P_{\rm ram}) \sim \frac{GM_{\rm BH}\rho_{\rm s}}{H}. \quad (3\cdot4)$$

Since the binding due to the gravitational force decreases as H increases, the disk expands preponderantly in the z-direction, forming strong shock waves (see the top

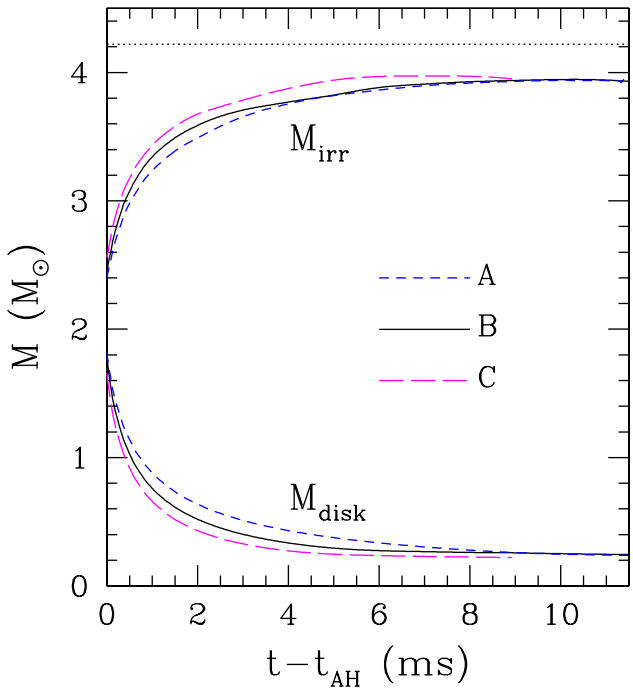

Fig. 3. Evolutions of the irreducible mass $M_{\rm irr}$ and the disk mass $M_{\rm disk}$. The long dashed, solid, and dashed lines represent the results for models A, B, and C, respectively. The horizontal line at $M \approx 4.2 M_\odot$ indicates the total mass.

right and middle left panels of Fig. 1). The propagation speed of the shock waves is $\approx 0.5c$, i.e., mildly relativistic. As the shock waves propagate, the mass accretion rate to the BH significantly decreases (see Fig. 3). After the shock propagation, a low density funnel region is formed around the rotational axis (see the middle right and bottom left panels of Fig. 1). In addition, the funnel region is surrounded by a dense, hot wall (see the bottom right panel of Fig. 1). The temperature in the funnel increases to approximately the same level as that in the wall through shock heating, and hence such a low density funnel can be supported by the thermal pressure.

Figure 2 displays the surface density, the optical depth, the temperature, and the angular velocity of the disk at $t = 290.14$ ms. Due to the shock heating, the temperature increases to $T \approx 4$–9×10^{10} K, which is about a factor of 4–5 larger than that in the unshocked regions (see the middle panel of Fig. 2). The surface density around the rotational axis is $\Sigma \approx 2$–6×10^{15}g/cm^2, while it is $\Sigma \sim 10^{17}$ g/cm^2 in the disk. This reflects the formation of the funnel structure formation (see the top panel of Fig. 2). Assuming that neutrino opacity is $\kappa_\nu = 7 \times 10^{-17} (T/10^{11}\,{\rm K})^2$ (see, e.g., Di Matteo et al. 2002), we compute the optical depth $\tau = \kappa_\nu \Sigma$. Then we find that the disk is optically thick for a radius of $R \approx 20$–130 km (see the top panel of Fig. 2). The subsequent evolution of the hot disk will be determined by the duration of the infall and the viscous timescale, as previously discussed (see, e.g., Ref. 39)).

Successful LGRB formation requires at least the following three ingredients: 1.

formation of an energetic fireball which yields highly relativistic outflows; 2. collimation of the relativistic outflows; 3. successful penetration of the outflows through a surrounding stellar mantle. As discussed in the following, all these conditions are likely to be satisfied in our model, even in the absence of a strong magnetic field, which is often assumed (see, e.g., Refs. 40) and 41)).

In our models, a highly relativistic fireball will be produced by the neutrino pair ($\nu\bar{\nu}$) annihilation around the rotational axis. Here, let us approximately estimate the energy deposition rate $\dot{E}_{\nu\bar{\nu}}$ through $\nu\bar{\nu}$ annihilation. In the diffusion limit, the neutrino flux is given by

$$F_\nu \approx \frac{7N_\nu}{3}\frac{\sigma T^4}{\kappa_\nu \Sigma}\,, \tag{3·5}$$

where $N_\nu = 3$ is the number of neutrino species and σ is the Stefan-Boltzmann constant. The neutrino luminosity from an optically thick disk is then

$$L_\nu \approx 2\pi R_{\rm disk}^2 F_\nu \sim 5\times 10^{53}\, T_{11}^2\, \Sigma_{17}^{-1} \left(\frac{R_{\rm disk}}{70\,{\rm km}}\right)^2 \ {\rm ergs/s}\,, \tag{3·6}$$

where $T_{11} \equiv T/10^{11}$ K and $\Sigma_{17} \equiv \Sigma/10^{17}$ g/cm^2. According to the results of Setiawan et al.,[42] the expected energy deposition rate through the $\nu\bar{\nu}$ annihilation would then be $\dot{E}_{\nu\bar{\nu}} \sim 10^{52}$ ergs/s. The low density funnel region above the BH will be a favorable place for an efficient production of ee^+ pairs through $\nu\bar{\nu}$ annihilation.

The formation of a dense, hot wall surrounding the funnel will play an important role in collimating relativistic outflows. In the absence of this wall, energetic outflows fail to be collimated, as the outflows travel through the stellar mantle. The shock waves formed at the birth of the BH are likely to sweep the matter along the rotational axis, reaching the stellar surface before the main relativistic outflows, which will be produced in the accretion phase (e.g., Ref. 39)), are driven.

For larger values of $|\Gamma_1 - 4/3|$, the time at the onset of the shock wave propagation is delayed, because the rate of increase of the disk pressure as well as the rate of decrease of the ram pressure is smaller, reflecting the less homologous nature of the collapse. This also results in the fact that it takes a longer time for the BH to relax to a stationary state (see Fig. 3). However this 'time delay' is at most ~ 10 ms for $\Gamma_1 \gtrsim 1.315$, and the features of the funnel structure formation are qualitatively the same for any of the adopted EOSs.

The thermal energy is stored in the inner part of the accretion disk if the heating timescale is shorter than the timescale of the neutrino cooling. The condition is $\alpha(GM\dot{m}/R) \gg L_\nu\,(\sim 10^{53}\,{\rm ergs/s})$, where $\alpha \lesssim 1$ is the effective conversion efficiency of the kinetic energy to the thermal energy through the shocks and $\dot{m}$ is the mass accretion rate. This gives $\dot{m} \gg L_\nu R/\alpha GM \approx \alpha^{-1} M_\odot\ {\rm s}^{-1}$. According to our results, $\dot{m} \gg 10 M_\odot\ {\rm s}^{-1}$ at least for $(t - t_{\rm AH}) \lesssim 10$ ms. Thus, the neutrino cooling does not play an important role in the thermal-energy-store phase, unless the conversion efficiency is extremely low, i.e., $\alpha \ll 0.1$. To summarize, our results are universal, at least qualitatively, for any of the EOSs and microphysical processes.

We also performed simulations for $0.8 \lesssim q \lesssim 1.2$, as well as for weakly differentially rotating cases and found essentially the same results for all these parameter

values. For larger values of $q \approx 1.2$, more collimated shock waves are formed. For smaller values of $q \leq 0.8$, a massive disk, which is essential for shock formation, is not formed. For sufficiently large values of $q > 1.2$, on the other hand, a BH is not promptly formed, due to the effect of the centrifugal force. In this case, a BH may be formed after a sufficient amount of angular momentum is transported.

The black hole excision technique enables us to continue the simulation until the BH has relaxed to a quasi-stationary state. As Fig. 3 shows, a seed BH with mass $M_{\rm irr} \approx 2.4 M_\odot$ is born at first for any of the EOSs. This value is approximately determined by the maximum allowed mass of the rigidly rotating configuration for the adopted EOSs. The figure also reveals that approximately 95% of the total mass is eventually swallowed by the BH for any of the adopted EOSs. Since the total angular momentum is conserved, the angular momentum of the BH can be indirectly estimated from that of the disk, which is $\sim 20\%$ of the total angular momentum. Thus, the final spin parameter of the BH is estimated as ≈ 0.8.

§4. Summary

Motivated by recently developed single-star evolutionary models of LGRB progenitors, we performed fully general relativistic simulations for rapidly rotating stellar core collapse to a BH. We found that a BH is directly formed as a result of the collapse of a sufficiently massive progenitor. Soon after the BH formation, a disk of density $\sim 10^{12}$ g/cm^3 is formed around the BH. The subsequent infall of matter from outside produces shocks at the surface of the disk, and thermal energy is generated, heating the disk. The thermal pressure eventually reaches $\sim 10^{31}$ dyn/cm^2, which is much larger than the ram pressure of the infalling matter, and hence it is used to sustain the vertical gravitational force. Because of the increasing thermal energy, the disk and shock front gradually expand, and when the scale height is comparable to the disk radius, the shock front starts to expand with mildly relativistic speed. The strong shock waves sweep matter around the rotational axis and heat up the disk matter to $\sim 10^{11}$ K. Then, a low-density ($\rho \lesssim 10^7$ g/cm^3) funnel region surrounded by a hot, dense wall is formed. Formation of such a structure in advance of the subsequent quasi-stationary accretion from the hot disk and the resulting relativistic outflows will be quite favorable for producing the fireball and LGRBs.

In the present simulation, we did not incorporate magnetic fields. It should be noted that even in the absence of magnetic stress, funnel structure, which will be essential for producing collimated jets, is formed. However, magnetic fields can further promote the formation of such a funnel if the field strength is larger than $\sim 10^{15}$ G (i.e., the magnetic pressure is larger than $\sim 10^{29}$ dyn/cm^2, which is comparable to the ram pressure of the infalling matter). Study of magnetic field effects is left as a future project.

Although our treatments of the EOS and microphysical processes in the present work are approximate, we believe that the qualitative features of the BH formation and subsequent shock formation found here will be universal. To confirm this process more rigorously, more detailed quantitative studies with a realistic EOS, including relevant microphysics, is needed. Such a study is in progress, and the results will be

reported in the near future.

Acknowledgements

We thank R. Takahashi and K. Maeda for valuable comments and discussions. Numerical computations were performed on the FACOM VPP5000 at the data analysis center of NAOJ and on the NEC SX-8 at YITP. This work is supported by JSPS Research Grant for Young Scientists (No. 1611308) and by Monbukagakusho Grant (No. 17030004).

References

1) J. Gorosabel et al., Astron. Astrophys. **400** (2003), 127.
2) L. Christensen, J. Hjorth and J. Gorosabel, Astron. Astrophys. **425** (2004), 913.
3) P. Jakobsson et al., Mon. Not. R. Astron. Soc. **362** (2005), 245.
4) T. J. Galama et al., Nature **395** (1998), 670.
5) S. R. Kulkarni et al., Nature **395** (1998), 663.
6) J. Hjorth et al., Nature **423** (2003), 847.
7) K. Z. Stanek et al., Astrophys. J. **591** (2003), L17.
8) K. S. Kawabata et al., Astrophys. J. **593** (2003), L19.
9) M. Modjaz et al., Astrophys. J. **645** (2006), L21.
10) J. Sollerman et al., Astron. Astrophys. **454** (2006), 503.
11) A. Zeh, S. Klose and D. H. Hartmann, Astrophys. J. **609** (2004), 952; in *Proc. 22nd Texas Symposium on Relativistic Astrophysics*, ed. P. Chen et al. (SLAC, Stanford, 2005).
12) S. E. Woosley, Astrophys. J. **405** (1993), 273.
13) B. Paczyński, Astrophys. J. **494** (1998), L45.
14) A. MacFadyen and S. E. Woosley, Astrophys. J. **524** (1999), 262.
15) W. Zhang and S. E. Woosley, Astrophys. J. **608** (2004), 365.
16) N. Langer, Astron. Astrophys. **329** (1998), 551.
17) P. Podsiadlowski et al., Astrophys. J. **607** (2004), L17.
18) C. L. Fryer and A. Heger, Astrophys. J. **623** (2005), 302.
19) S.-C. Yoon and N. Langer, Astron. Astrophys. **443** (2005), 643; in *ASP Conf. Ser., Stellar Evolution at Low Metallicity: Mass-Loss, Explosions, Cosmology*, ed. H. Lamers et al. (ASP, San Francisco, 2006); astro-ph/0511222.
20) S.-C. Yoon, N. Langer and C. Norman, Astron. Astrophys. **460** (2006), 199.
21) S. E. Woosley and A. Heger, Astrophys. J. **637** (2006), 914; in *AIP Conf. Proc., Gamma Ray Bursts in the Swift Era*, ed. S. S. Holt, N. Gehrels and J. Nousek (ASP, San Francisco, 2006); astro-ph/0604131.
22) J. S. Vink and A. de Koter, Astron. Astrophys. **442** (2005), 587.
23) A. Maeder, Astron. Astrophys. **178** (1987), 159.
24) J. P. U. Fynbo et al., Astron. Astrophys. **406** (2003), L63.
25) R. L. C. Starling et al., Astron. Astrophys. **442** (2005), L21.
26) J. Gorosabel et al., Astron. Astrophys. **444** (2005), 711.
27) K. Z. Stanek et al., Acta Astron. **56** (2006), 333.
28) S. L. Shapiro and S. A. Teukolsky, *Black Holes, White Dwarfs, and Neutron Stars* (Wi1ey interscience, New York, 1983).
29) T. Zwerger and E. Müller, Astron. Astrophys. **320** (1997), 209.
30) K. Nakazato, K. Sumiyoshi and S. Yamada, Astrophys. J. **645** (2006), 519.
31) D. J. Nice et al., Astrophys. J. **634** (2005), 1242.
32) T. Di Matteo, R. Perna and R. Narayan, Astrophys. J. **579** (2002), 706.
33) M. Shibata, Phys. Rev. D **67** (2003), 024033.
34) M. Alcubierre and B. Brügmann, Phys. Rev. D **63** (2001), 104006.
35) M. Shibata and K. Taniguchi, Phys. Rev. D **73** (2006), 064027.
36) M. Shibata, M. D. Duez, Y. T. Liu, S. L. Shapiro and B. C. Stephens, Phys. Rev. Lett. **96** (2006), 031102.
37) M. Shibata and S. L. Shapiro, Astrophys. J. **572** (2002), L39.

38) W. H. Lee and E. Ramirez-Ruiz, Astrophys. J. **641** (2006), 961.
39) W. H. Lee, E. Ramirez-Ruiz and D. Page, Astrophys. J. **632** (2005), 421.
40) D. Proga et al., Astrophys. J. **599** (2003), L5.
41) T. Takiwaki et al., Astrophys. J. **616** (2004), 1086.
42) S. Setiawan, M. Ruffert and H.-Th. Janka, Mon. Not. R. Astron. Soc. **352** (2004), 753; Astron. Astrophys. **458** (2006), 553.